The effects of ground-state dynamics on the emission spectra of electric-discharge-pumped XeCl lasers: A model for injection locking

Mieko Ohwa and Mark J. Kushner[a)]
University of Illinois, Department of Electrical and Computer Engineering, Gaseous Electronics Laboratory, 607 East Healey, Champaign, Illinois 61820

(Received 28 November 1988; accepted for publication 1 February 1989)

The bandwidth of excimer lasers is typically 1–10 Å as a result of their transitions being multiline or bound-free. To obtain high power with narrow bandwidth injection locking is usually required. In this paper, we investigate the spectral characteristics of electric-discharge-pumped XeCl ($B \rightarrow X$) lasers during injection locking and free-running operation. This study is performed using results from an electron kinetics and plasma chemistry model for Ne/Xe/HCl/H_2 mixtures which includes multiline laser extraction. We find that the experimentally observed lasing spectrum cannot be explained if a thermal distribution is used for the vibrational levels of the X state. Therefore, the vibrational levels of the B, C, and X states are explicitly included in the model and the gain spectrum is computed using Franck–Condon factors. Results from the model indicate that bottlenecking occurs on the $v' = 0 \rightarrow v'' = 1$ transition, while the dissociation rate for $XeCl(X,v'' = 2)$ is faster than the removal rate for $XeCl(X,v'' = 1)$. Injection locking characteristics are examined as a function of injection intensity and small-signal gain. Due to nonequilibrium dynamics in the ground state, locking efficiency does not necessarily increase with increasing small-signal gain.

I. INTRODUCTION

While KrF and ArF $B \rightarrow X$ excimer lasers operate on bound-free transitions, XeF and XeCl $B \rightarrow X$ excimer lasers operate on bound-bound transitions. The binding energy of $XeF(X)$ is ≈ 1000 cm^{-1} while that of $XeCl(X)$ is ≈ 200 cm^{-1}.[1,2] The rates of collisional decay for the low-lying vibrational levels of the X state are therefore important in determining the spectrum and efficiency of XeF and XeCl. XeCl lasers can be operated with long optical pulses (> 10 ns) which implies that the rate of removal of population in the X state must be commensurate with the rate of population of that state by optical saturation. Given typical rate constants for electron and heavy particle reactions, only collisions with the buffer gas are frequent enough to be responsible for the observed rate of quenching of $XeCl(X)$.

Removal of population from specific vibrational levels in the X state of XeCl occurs dominantly by two processes. Vibrational-translational (VT) collisions redistribute the population of the X state among the vibrational levels while collisional dissociation directly removes population from the X state. Fulghum, Feld, and Javan have experimentally studied the collisional decay rates for low-lying vibrational levels of $XeF(X)$.[3] They concluded that the VT processes rapidly equilibrate the X-state vibrational manifold. The different vibrational levels were found to decay at a common rate with dissociation primarily occurring from the highest vibrational levels. Although no definitive similar measurements have been reported for $XeCl(X)$, vibrational relaxation and thermalization of the vibrational levels of $XeCl(X)$ are usually assumed to occur on a time scale that is less than the effective lifetime of the upper laser level.[4,5] This assumption is based on the fact that the vibrational level spacing in the X state (≈ 20 cm^{-1})[6] is small compared to kT_g (T_g is the gas temperature). For this reason, one would also expect $XeCl(X)$ to collisionally dissociate at a rate which is close to the gas kinetic rate since the dissociation energy is commensurate with kT_g. This assumption requires close coupling between the internal and translational modes of $XeCl(X)$. Early experiments, though, indicated that the decay rates for low-lying vibrational levels of $XeCl(X)$[7] may be too slow to enable the XeCl laser to operate with the observed efficiencies.[8,9] Although these early results are not totally conclusive, the assumption that the vibrational distribution of $XeCl(X)$ is in thermal equilibrium may be suspect.

In high-pressure gas mixtures (> 1 atm) the strongest $XeCl(B \rightarrow X)$ laser lines are four vibrational transitions near 308 nm which originate from $XeCl(B,v' = 0)$ and terminate on the $v'' = 0$, 1, 2, and 3 vibrational levels of $XeCl(X)$.[2,4] At high pressures, the vibrational distribution of $XeCl(B,v')$ is often assumed to be in an equilibrium Boltzmann distribution at the gas temperature.[2] Corkum and Taylor, though, have inferred the populations of $XeCl(B,v' = 0,1)$ from gain spectra they measured in a discharge-pumped XeCl laser.[4] They concluded that the vibrational temperature of the B state would need to be far in excess of the gas temperature if the vibrational distribution was thermally distributed. Similar gain spectra for a discharge-pumped XeCl laser have been reported by Bourne and Alcock.[5] Total gain and efficiency of $XeCl(B \rightarrow X)$ lasers will logically depend on the vibrational distribution of $XeCl(B,v')$ and the fraction of B-state population in $v' = 0$. The laser spectrum, however, does not directly depend on the vibrational distribution in the B state since all transitions of interest originate on $XeCl(B,v' = 0)$. The spectrum, rather, depends on the oscillator strengths of the transitions and the vibrational distribution of population in $XeCl(X,v'')$. Consequently, the dynamics of the redistribution of population in the ground state is the key factor in determining the lasing spectra of XeCl lasers.

In this paper we examine the effect of the rates of colli-

a) Author to whom correspondence should be addressed.

 0021-8979/89/114138-12$02.40

sional dissociation for low-lying vibrational levels of XeCl(X,v'') and the rate of vibrational thermalization of the XeCl(X,v'') on the lasing spectra of electric-discharge-pumped XeCl($B\rightarrow X$) lasers. This study is performed with results from a computer model for electric-discharge-pumped XeCl lasers using Ne/Xe/HCl/H_2 mixtures. The model includes an electrical discharge circuit and the pertinent heavy particle and electron collision processes as do other excimer laser models. We have improved upon those models by vibrationally resolving the B, C, and X states, by calculating the wavelength dependence of the gain near 308 nm, and by including multiline laser extraction. The gain spectrum is calculated using Franck–Condon factors and the vibrational-rotational populations in the upper and lower laser levels.

Part of the motivation for this study was to identify the optimum conditions for injection locking discharge pumped XeCl($B\rightarrow X$) lasers. Injection locking is effective in producing high-power radiation having a narrow bandwidth from sources which oscillate free-running with a broadband spectrum. This technique involves injecting the output of a narrow-band low-power source into the optical cavity of a broadband high-power laser. The injected signal provides a spectral mode which, in principal, should dominate over those modes which would otherwise build up from spontaneous emission. Consequently, the increase in intensity for the injected mode is larger than the others. The rate of increase, though, is strongly dependent on the injection intensity and the small-signal gain of the active medium. If the injected mode saturates the spectral properties of the active medium may then begin to dominate, and the laser may revert to its free-running spectrum. To investigate these issues injection locking characteristics of discharge-pumped XeCl($B\rightarrow X$) lasers were analyzed as a function of injection intensity and small-signal gain based on calculation of the dynamic gain spectrum. Computed spectral characteristics were compared to the experimental results of Bourne and Alcock.[5] We find that in order to explain the observed spectral characteristics of discharge pumped XeCl lasers, the vibrational distribution of the X state cannot be assumed to be in thermal equilibrium and, in fact, significant bottlenecking must occur.

The model is described in Sec. II, followed by a discussion of computed laser spectra in Sec. III. The characteristics of injection-locked lasers are discussed in Sec. IV, and the dependence of those characteristics on gain and position in the discharge are discussed in Secs. V and VI. Concluding remarks are in Sec. VII.

II. DESCRIPTION OF THE MODEL

The model used in this study is based on those reported in Refs. 10 and 11 for discharge-pumped XeCl($B\rightarrow X$) lasers. The model for the discharge circuit using spikers and magnetic diodes and the method of incorporation of the electron impact rate coefficients into the kinetics were taken from Ref. 10. The heavy particle reaction scheme and rate coefficients are based on those from Ref. 11. As improvements to those models, we also include reactions in the plasma kinetics relating to H_2 to carefully treat the effect of HCl depletion on laser performance which occurs during long pumping. We also explicitly included the vibrational levels of the XeCl B, C, and X states, and included an analysis of the laser spectrum. Multiwavelength laser extraction is also accounted for. The spectrum of the laser gain is dominated by vibrational relaxation in both the upper and lower laser levels, and dissociation in the lower laser level. Since these processes are strongly dependent on the gas temperature, we also included gas temperature as a variable.

The structure of our model is similar to that of models for discharge-pumped XeCl($B\rightarrow X$) lasers previously reported and therefore will only be briefly reviewed.[8,11,12] The model consists of three submodels for the electrical discharge circuit, heavy particle and electron collision kinetics in the plasma, and optical extraction. The rate constants for electron collision processes are calculated by solving Boltzmann's equation for the electron distribution function including electron-electron collisions and superelastic collisions. The numerical procedure for solving Boltzmann's equation is basically the same as that reported by Johnson, Palumbo, and Hunter.[13] Operationally, Boltzmann's equation is solved offline and parametrized as a function of gas mixture, E/N, electron density, and excitation density. The resulting electron impact rate coefficients and transport coefficients are placed in a multidimensional look-up table which is interpolated during execution of the code.

A. Processes relating to XeCl(B)

In order to accurately represent the gain dynamics in high pressure XeCl($B\rightarrow X$) discharge lasers, it is necessary to obtain the population for XeCl($B,v'=0$). This value is determined by the combined effects of the excitation rates for the B and C states, the vibrational relaxation within both the B and C states, mixing of the B state with the C state, collisional quenching, and stimulated emission. The branching ratios for the initial distribution of XeCl(B) and XeCl(C) from excitation reactions was obtained from the results of kinetic studies of electron-beam-pumped Ne/Xe/HCl and Ar/Xe/HCl gas mixtures.[14,15] The branching ratios of XeCl(B) and XeCl(C) obtained from these studies are 0.77 and 0.23, respectively, and we used these values in the model. Since excitation in both e-beam and discharge-pumped lasers is dominated by ion-ion neutralization (e.g., $Xe^+ + Cl^- + Ne \rightarrow XeCl^* + Ne$) the use of branching ratios derived from e-beam excitation are likely to be valid.[8,9,11,12]

State-to-state relaxation processes forXeCl(B,C) have been experimentally investigated in low-pressure mixtures. The results indicate that the rates of vibrational relaxation in the B state, and of mixing between the B and C vibrational levels, increase with increasing vibrational level. These rates are not fast enough in Ne buffers, though, to be treated as an instantaneous relaxation to thermal equilibrium.[16,17] From an analysis of the fluorescence of $B\rightarrow X$ and $C\rightarrow A$ transitions in low-pressure mixtures, Dreiling and Setser concluded[16] that the vibrational relaxation rate in Ar buffers can be approximated as increasing exponentially with increasing vibrational level. In this approximation the probability for vibrational relaxation scales as $\exp[-(b\Delta\epsilon/kT_g)]$ where $\Delta\epsilon$

is the energy separation between the vibrational levels and b is a semiempirical factor (0.11 for Ar collisions).

The vibrational spacing for the B state has been experimentally measured as ≈ 195 cm^{-1} by Sur, Hui, and Tellinghuisen.[6] No experimental value for the C state has been reported though a value of 188 cm^{-1} has been reported based on an *ab initio* calculation.[18] The vibrational energy spacing for the B and C states in the model was taken as 195 and 188 cm^{-1}, respectively. From an analysis of the fluorescence intensities for $B \rightarrow X$ and $C \rightarrow A$ transitions, the B-C energy separation has been estimated to be $E_B - E_C = 128$, 220, and 280 cm^{-1} by Tellinghuisen and McKeever,[19] Brashears, Setser, and Yu,[20] and Lo and Zheng,[21] respectively. The B-C energy separation is therefore approximately equal to the vibrational spacing in the B and C states and approximately equal to kT_g.[9,16] The uncertainty in the value of the B-C energy separation is therefore expected to exert little influence on the vibrational distribution among the lowest vibrational levels since there is not a large activation energy barrier to overcome. In this work we chose $E_B - E_C = 200$ cm^{-1}.

To account for vibrational relaxation and mixing in the model we resolved the B and C states into five vibrational levels ($v' = 0$–4). Quenching reactions out of XeCl(B,v') and XeCl(C,v') are identical for all vibrational levels and are listed in Table I. Working on the assumption that excitation of the B and C states occurs high in their vibrational manifolds, we have all excitation feed XeCl(B,$v' = 4$) and XeCl(C,$v' = 4$).[24] This assumption is equivalent to having an instantaneous relaxation to $v' = 4$ within the B and C states without mixing between them. Mixing between XeCl(B,v') and XeCl(C,v') was treated as follows. For the $v' = 0$, 1, 2, and 3 levels of XeCl(B,v'), exchange occurs with the $v' + 1$ level of the C state:

$$\mathrm{XeCl}(B,v') + \mathrm{Ne} \rightleftarrows \mathrm{XeCl}(C,v'+1) + \mathrm{Ne}. \quad (1)$$

Exchange occurs directly between the $v' + 4$ level of the B and C states to account for exchange between higher vibrational levels,

$$\mathrm{XeCl}(B,v'=4) + \mathrm{Ne} \rightleftarrows \mathrm{XeCl}(C,v'=4) + \mathrm{Ne}. \quad (2)$$

A rate constant of 4.8×10^{-12} cm^3 s^{-1} was used for all exothermic vibrational exchange reactions.[16] Detailed balance based on the gas temperature was used to obtain the reverse rates. Recent measurements of the fluorescence intensity ratio of $B \rightarrow X$ and $C \rightarrow A$ transitions at high current densities in discharge-pumped XeCl lasers have shown that electron collision mixing is insignificant at high gas pressures.[21] Therefore, electron collision mixing of the B and C states was not included in the model. The rate constants used in the model for collisional relaxation by neon ($v' \rightarrow v' - 1$) in both XeCl(B) and XeCl(C) are 7.3×10^{-12} cm^3 s^{-1} for $v' \leqslant 3$ and 1.5×10^{-11} cm^3 s^{-1} for $v' = 4$. The rate constants for reverse reactions ($v' \rightarrow v' + 1$) were obtained by detailed balance based on the gas temperature. Collisional relaxation by two and three quanta was also included using rate constants having values 0.9 and 0.8, respectively, of that for the single quanta relaxation as given by energy gap scaling. The vibrational relaxation and B-C mixing due to collisions with Xe are treated similarly to that for Ne using the rate constants reported in Ref. 23. The rate constant used for B-C mxing by collisions with xenon is 1.1×10^{-10} cm^3 s^{-1}. Collisional relaxation by xenon within the B and C states proceeds with rate constants of 2.0×10^{-10} cm^3 s^{-1} for $v' \leqslant 3$ and 4.0×10^{-10} cm^3 s^{-1} for $v' = 4$.

The main pathways resulting in the production of the XeCl* excimer in discharges and e beams are fairly well understood.[8–12,25] The dominant processes for formation of XeCl* are three-body ion-ion neutralization reactions such as

$$\mathrm{Xe}^+ + \mathrm{Cl}^- + \mathrm{Ne} \rightarrow \mathrm{XeCl}^* + \mathrm{Ne}, \quad (3)$$

$$\mathrm{NeXe}^+ + \mathrm{Cl}^- + \mathrm{Ne} \rightarrow \mathrm{XeCl}^* + \mathrm{Ne} + \mathrm{Ne}, \quad (4)$$

where Cl^- is predominantly formed by the dissociative attachment of electrons to vibrationally excited HCl($v = 1,2$). Since lean mixtures (Xe mole fraction $< 1\%$ and HCl fractions $\leqslant 0.1\%$) as are usually used for discharge-pumped XeCl lasers, the ion-ion neutralization reaction

$$\mathrm{Xe}_2^+ + \mathrm{Cl}^- + \mathrm{Ne} \rightarrow \mathrm{XeCl}^* + \mathrm{Xe} + \mathrm{Ne} \quad (5)$$

and the neutral harpooning processes such as

$$\mathrm{Xe}^* + \mathrm{HCl}(v = 1,2) \rightarrow \mathrm{XeCl}^* + \mathrm{H} \quad (6)$$

contribute little to the formation of XeCl*, even at high pressures (> 1 atm). In any XeCl* formation processes HCl is required as a feedstock, either directly or as the precursor to Cl^-. For long pumping times, the depletion of the HCl molecule will therefore be important. The reactions which replenish the HCl, such as

TABLE I. Rate constants for XeCl* quenching.

Process	Rate constant[a]	Reference
XeCl* + Ne → Xe + Cl + Ne	1.0(−14)	Estimated
XeCl* + Xe → Xe + Cl + Xe	2.1(−12)	22
XeCl* + HCl → Xe + Cl + HCl	6.3(−10)	23
XeCl* + HCl($v = 1$) → Xe + Cl + HCl	6.3(−10)[b]	
XeCl* + HCl($v = 2$) → Xe + Cl + HCl	6.3(−10)[b]	
XeCl* + Cl_2 → Xe + Cl + Cl + Cl	4.3(−10)	23
XeCl* + Ne + Ne → Xe + Cl + Ne + Ne	1.0(−34) cm^6 s^{-1}	Estimated
XeCl* + Xe + Xe → Xe_2Cl^* + Xe	4.0(−31) cm^6 s^{-1}	15
XeCl* + Xe + Ne → Xe_2Cl^* + Ne	5.0(−32) cm^6 s^{-1}	Estimated
XeCl* + e → Xe + Cl + e	1.0(−7)	15

[a] cm^3 s^{-1} unless otherwise noted.
[b] Analogy to XeCl* + HCl.

$$Cl + H + Ne \rightarrow HCl + Ne, \quad (7)$$

are so slow (5.5×10^{-32} cm^6 s^{-1}) that HCl will be consumed as the discharge proceeds. Depletion of HCl decreases the XeCl* formation rate and increases the rate of collision quenching due to the increase in electron density which is caused by the reduction of the attaching species.

Hydrogen, often used as a trace additive to XeCl gas mixtures, can influence the HCl balance as well as the electron kinetics. Adhkamov *et al.*[26] performed a parametric study on the effect of H_2 addition on laser performance. They observed an imrovement in the laser output energy as well as an improvement in reproducibility from one pulse to another. They proposed that cooling of electrons due to vibrational excitation of H_2 increases the rate of vibrational excitation of HCl by better matching of the electron distribution function to those cross sections and by the exchange reaction

$$H_2(v=1) + HCl \rightarrow HCl(v=1,2) + H_2. \quad (8)$$

The increased density of HCl(v) leads to dissociative attachment and harpooning reactions which are the precursors to XeCl*. Even for mixtures which do not initially include H_2, the molecule will be generated by the reaction

$$H + H + Ne \rightarrow H_2 + Ne \quad (9)$$

though this is also a slow process. To account for these processes we included the vibrational excitation, relaxation, and dissociation of H_2. We used a rate constant of 6.0×10^{-11} cm^3 s^{-1} for reaction (8) with equal branching to HCl($v=1,2$).

B. Gain spectrum

The model for the gain spectrum used in this work for XeCl($B\rightarrow X$) emission is similar to that reported by Adamovich *et al.*[27] In the model the gain at frequency ν, $g(\nu)$, is given by

$$g(\nu) = \sum_{v''=0}^{3} \sum_{J}^{J_{\max}} (F_P^{v'',J} + F_R^{v'',J}), \quad (10)$$

$$F_{P,R}^{v'',J} = K \frac{c^2}{8\pi^2\nu^2} \frac{J}{\tau} \left[\frac{[\mathrm{XeCl}(B,v'=0)]}{Q_B} \times \exp\left(\frac{-B'J(J\mp1)}{kT_g}\right) - \frac{\mathrm{XeCl}(X,v'')}{Q_C} \times \exp\left(\frac{-B''J(J\pm1)}{kT_g}\right)\right] \times f(v'=0,v'',J) \frac{\gamma}{\gamma^2 + (\Delta\nu_{P,R})^2}, \quad (11)$$

$$K = \begin{cases} 1 & (1 \leqslant J < 20) \\ \frac{1}{4} & (J \geqslant 20) \end{cases},$$

$$\Delta\nu_{P,R} = [E_B - E_X + B'J(J\mp1) - B''J(J\pm1)]/h - \nu, \quad (12)$$

where γ is the broadening coefficient, τ is the radiative lifetime, $Q_{B,C}$ are the rotational partition functions, and $E_{B,X}$ are the absolute (including electronic) energies of the vibrational levels. P and R refer to the rotational transitions of $J\rightarrow J+1$ and $J\rightarrow J-1$, respectively. $f(v',v'',J)$ are the Franck–Condon factors and the broadening coefficient was 4×10^9 atm s^{-1}. The contributions of rotational levels up to dissociation limit ($J\approx60$) for the P and R branches are taken into account. Rotational constants were obtained from Sur, Hui, and Tellinghuisen.[6] A value of $B' = 0.0669$ cm^{-1} was used for all levels of XeCl(B). For XeCl(X,v'') we used $B' = 0.056$ cm^{-1} for XeCl($X,v''=0$) and $B' = 0.0274$ cm^{-1} for XeCl ($X,v''=12$). Intermediate values were obtained by linear interpolation. Franck–Condon factors we obtained from the calculations of Sur, Hui, and Tellinghuisen[6] assuming rotational thermalization in both the B and X states. As Franck–Condon factors were only available for $J=0$ and $J=50$, factors for intermediate values of J were obtained by linear interpolation.

III. LASER SPECTRA AND DENSITIES OF XeCl($B,C,X;v$)

In this section we will discuss simulated laser spectra for the XeCl($B\rightarrow X$) transition and their relation to the distribution of vibrational levels in XeCl B, C and X states. To check the validity of our model we compared our results to the experiments reported by Fisher *et al.*[10] Their laser discharge had a 3.8 cm high by 3 cm wide by 60 cm long volume and used a spiker-magnetic diode circuit. The optical cavity consisted of a maximum reflector and a 20% reflectivity output mirror separated by 1.05 m. The gas mixture was Ne/Xe/HCl = 99.47/0.5/0.03 at 5 atm. With 70.7 J stored on the spiker and pulse forming line, the output energy was as much as 2.6 J with a pulse width of $\approx$150 ns. Our model predicts a total laser output energy of 2.8 J with an overall efficiency of 3.9% which agrees well with experiments. The computed efficiency results from an energy deposition efficiency of 85% and an intrinsic laser efficiency of 4.5%. The intrinsic efficiency is the product of a formation efficiency of 12% and an extraction efficiency of 39%. The calculated peak pumping density is 0.4 MW cm^{-3} which is obtained at $\approx$150 ns after breakdown of the gas.

Time histories of the vibrational populations of the upper laser level (B and C) for the discharge conditions of Fisher *et al.*[10] are shown in Fig. 1 without lasing. The level having the maximum density in each state is $v=0$ even though excitation of XeCl* initially forms in $v=4$, thereby indicating rapid vibrational relaxation compared to the rate of quenching and radiative decay. The total populations in XeCl(B) and XeCl(C) are similar with the total density in XeCl(C) being approximately 25% larger even though formation of XeCl* favors XeCl(B). This condition results, in part, from the higher rate of spontaneous emission from XeCl(B). The tight coupling between XeCl(B) and XeCl(C) by v-v exchange, and the fact that the C state is energetically lower than the B state would, by themselves, result in larger equilibrium density in XeCl(C).

The calculated small-signal gain spectra near 308.0 nm for the pumping conditions of Fisher *et al.* are shown in Fig. 2. For these results we assumed that the vibrational distributions in the B and X states are in equilibrium. The total densities of XeCl(B) and XeCl(X) are 2×10^{14} and 1×10^{13} cm^{-3}, respectively. The total gas pressure is 5 atm, and we show spectra for different gas temperatures. High gas temperatures, as may occur with prolonged pumping, reduce

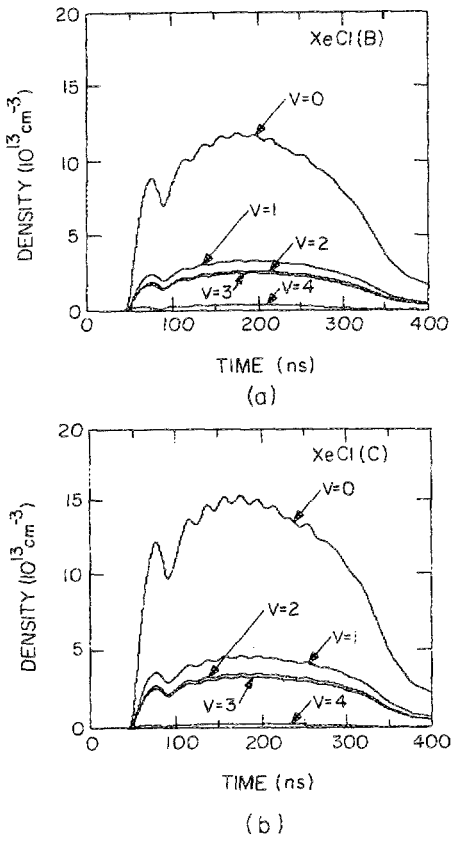

FIG. 1. Densities of the vibrational levels in the (a) B state and (b) C state of XeCl during the current phase through a discharge excited Ne/Xe/HCl = 99.47/0.5/0.03 mixture. The pressure is 5 atm and the average power deposition is 400 kW cm^{-3}. The densities of the $v = 4$ level in both the B and C states are intended to represent the density of that level and all higher-lying vibrational levels. Formation of XeCl(B) and XeCl(C) therefore occurs in $v = 4$ as an approximation to excitation occurring in highly excited vibrational levels.

peak gain at the laser wavelengths. This effect is due primarily to a redistribution of population in the upper laser level to higher vibrational and rotational levels. We also find that the decrease in gain increases with increasing wavelengths. This effect results from the rotational distribution for the higher

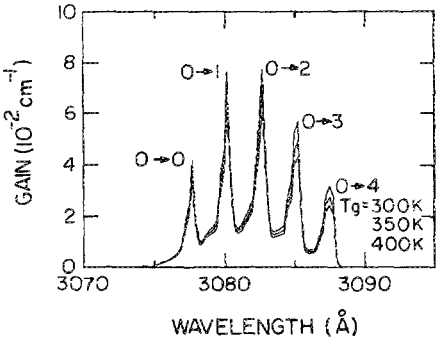

FIG. 2. Synthesized gain spectrum for the XeCl($B \rightarrow X$) transition at gas temperatures of 300, 350, and 400 K. The transitions are for XeCl($B, v' = 0$) → XeCl($X, v'' = 0,1,2,3$) progressing from lower to higher wavelength. For this example, the rotational and vibrational distributions are assumed to be in equilibrium with the gas temperature. Gain decreases with increasing gas temperature due to shifting of population to higher rotational states.

vibrational levels of XeCl(X) being more sensitive to the gas temperature due to their smaller rotational constants.

In their study of the spectra discharge-pumped XeCl($B \rightarrow X$) lasers Bourne and Alcock found that the output energy in the free-running system is nearly equally divided between $0 \rightarrow 1$ and $0 \rightarrow 2$ transitions.[5] [The notation $v' \rightarrow v''$ refers to the XeCl(B,v') → XeCl(X,v'') transition.] Both of the lines reach threshold and terminate at the same time. They also found that when injection locking the laser, the percentage of energy extracted at the injected wavelength is strongly dependent on wavelength. The locking efficiency (fraction of total laser energy at the injected wavelength) dropped off rapidly as the injection source was tuned away from the two free-running transitions ($0 \rightarrow 1$, $0 \rightarrow 2$). When the injected signal was tuned away from these transitions, laser oscillation initially occurred at the injected wavelength and subsequently reverted to the $0 \rightarrow 1$ and $0 \rightarrow 2$ transitions. Bourne and Alcock suggested that when modeling a free-running XeCl laser system the two lines $0 \rightarrow 1$ and $0 \rightarrow 2$ should be given approximately equal weight.[5] Lyutskanov, Khristov, and Tomov also measured the laser energy spectrum and found that in the free-running oscillator the $0 \rightarrow 1$ and $0 \rightarrow 2$ transitions are approximately equal in energy.[28] We will find that the time dependence of the spectrum of an injection-locked laser depends strongly on the degree of saturation of the XeCl($B, v' = 0$) level and the redistribution of population in the vibrational levels of the X state.

Calculated time histories of laser power and gain for the $v' = 0 \rightarrow v'' = 0$, 1, 2, and 3 transitions are shown in Fig. 3 for a free-running system. For these results we assumed that the vibrational distribution in the X state is in thermal equilibrium at T_g. The pumping and cavity conditions are the same as the experiments of Fisher *et al.*[10] Laser oscillation for each $B \rightarrow X$ vibrational transition is assumed to occur at the wavelength for which gain is maximum, and the gain shown in Fig. 3(b) are for these wavelengths. Note that the $0 \rightarrow 1$ transition dominates. Using the self-consistent oscillator strengths obtained from our analysis incorporating Franck–Condon factors, these results are not consistent with the observation that the laser output energy for the $0 \rightarrow 1$ and $0 \rightarrow 2$ should be approximately equal. Both of the lines, though, build up and terminate at the same time as observed experimentally. Gain on the $0 \rightarrow 1$ transition is slightly higher than that on the $0 \rightarrow 2$ transition both before and during laser oscillation [see Fig. 3(b)], and the intensity for that transition is preferably amplified. In order to explain the experimentally observed ratio of laser energy between the $0 \rightarrow 1$ and $0 \rightarrow 2$ transitions while using our self-consistent gain spectrum, the saturation intensity for the $0 \rightarrow 1$ transition must be lower than that for the $0 \rightarrow 2$ transition. Since these transitions share the same upper level, the decay time for the XeCl($X, v'' = 1$) vibrational level must then be longer than that for the XeCl($X, v'' = 2$) level; that is, bottlenecking must occur on the $0 \rightarrow 1$ transition.

In order to introduce the necessary bottlenecking on the $0 \rightarrow 1$ transtion into the gain spectrum, we modeled the X state conceptually having eight effective species. Four species represent the density of XeCl(X, v''), $v'' = 0$, 1, 2, and 3 which would result from being in equilibrium with the in-

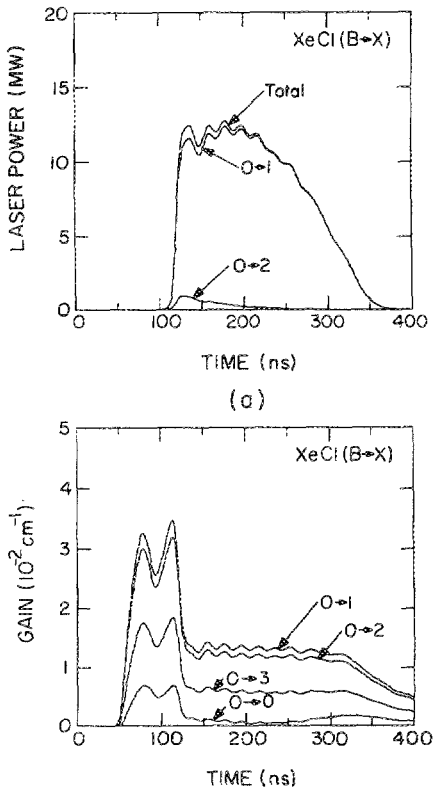

FIG. 3. Lasing and gain characteristics for a free-running XeCl($B\rightarrow X$) oscillator when the vibrational states in the XeCl(X) state are in equilibrium with the gas temperature: (a) laser intensity on the $0\rightarrow 1$ and $0\rightarrow 2$ transitions and (b) gain on the $0\rightarrow 0$, 1, 2, and 3 transitions. For these conditions, oscillation on the $0\rightarrow 1$ transition dominates. The $0\rightarrow 2$ transition oscillates only early during the pulse prior to saturation. These results do not agree with experiments in which power is more evenly divided between the $0\rightarrow 1$ and $0\rightarrow 2$ transitions. This implies that bottlenecking must occur in the XeCl($X,v''=1$) level.

stantaneous gas temperature based on the total density of the X state in the absence of optical transitions. Four additional species account for the nonequilibrium populations for XeCl(X,v''), $v''=0$, 1, 2, and 3 resulting from optical transitions. Depopulation of these levels is by direct dissociation and relaxation to the equilibrium distribution. The use of this representation for XeCl(X,v'') is based on the observations of Fulghum and co-workers[3] for the method of decay of XeF(X,v''). They found that the vibrational levels thermally equilibrated fairly rapidly and that the vibrational levels decay with a common rate. The relaxation of the nonequilibrium vibrational densities to their instantaneous equilibrium value approximates this rapid intralevel equilibration. The densities of both the nonequilibrium and equilibrium components are used to calculate the gain.

The rate constant for the direct dissociation of the nonequilibrium XeCl($X,0\leqslant v''\leqslant 4$) is based on those used by Fulghum, Feld, and Jaran for XeF(X),[29]

$$k_i = C_D \exp(\beta E_i/D_0)\exp[-(D_0-E_i)/kT], \quad (13)$$

where E_i is the energy of the vibrational level, D_0 is the dissociation energy of the X state, and C_D and β are constants. We adjusted C_D and β in our model to match the spectral characteristics reported by Bourne and Alcock.[5] We also parametrized the rate constant for vibrational thermalization k_V and effective dissociation rate constant k_D for the portion of X-state population which is in equilibrium with the ambient gas temperature. The values so derived are not unique. However, they must satisfy the condition that the dissociation rate for XeCl($X,v''=2$) is faster than the removal rate for the $v''=1$ level. We find that the lasing spectra are sensitive to our choices of β and k_V. For $10\leqslant\beta\leqslant 20$, we may reproduce the spectral characteristics obtained by Bourne and Alcock[5] by adjusting k_V to be within the range of $1\times 10^{-12}\leqslant k_V\leqslant 1\times 10^{-11}$ cm^3 s^{-1}. Our choices of k_V and k_D were based on matching these experimental results. The results in the remainder of this paper were obtained with $C_D=7.8\times 10^{-12}$ cm^3 s^{-1}, $\beta=10$, $k_V=1\times 10^{-12}$ cm^3 s^{-1}, and $k_D=4\times 10^{-11}$ cm^3 s^{-1}. The rate constant k_V characterizes the rate at which the nonequilibrium distribution relaxes to the equilibrium distribution. Since many collisions may be required for total relaxation, one would expect k_V to be less than the gas kinetic rate constant.

Laser power and gain for the XeCl($B\rightarrow X$) transitions in free-running system are shown in Fig. 4 using our derived rate constants. The calculated output energy is 2.8 J of which 34% is on the $0\rightarrow 1$ transition. These spectral characteristics for a free-running system are in good agreement with the

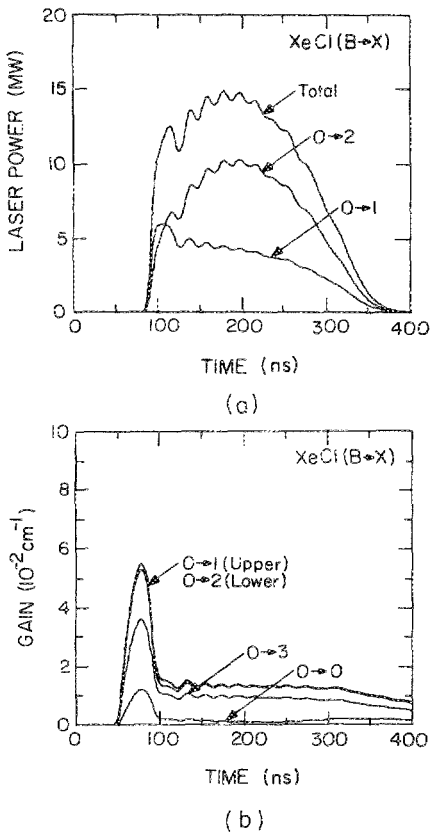

FIG. 4. Lasing and gain characteristics for a free-running XeCl($B\rightarrow X$) oscillator when the vibrational states in the XeCl(X) are given by their nonequilibrium kinetics; (a) laser intensity on the $0\rightarrow 1$ and $0\rightarrow 2$ transitions and (b) gain on the $0\rightarrow 0$, 1, 2, and 3 transitions. The conditions are otherwise the same as for Fig. 3. To obtain roughly equal laser power on the $0\rightarrow 1$ and $0\rightarrow 2$ transitions, the rate of clearing of XeCl($X,v''=2$) must be greater than that for XeCl($X,v''=1$). With nonequilibrium kinetics in the X state the small-signal gain prior to oscillation is nearly equal for the $0\rightarrow 1$ and $0\rightarrow 2$ transitions.

experimental results of Bourne and Alcock.[5] In comparing these results with the case where we assumed vibrational thermalization in the X state, we find that the gains for $0\rightarrow 1$ and $0\rightarrow 2$ transitions are more closely equal. Also both of the lines build up and terminate at the same time. When gain of the $0\rightarrow 1$ transition drops due to saturation and bottlenecking, the gain on the $0\rightarrow 2$ transition is higher than that of the $0\rightarrow 1$ transition. The time dependence of gain for the two lines, though, is identical after saturation of the $0\rightarrow 2$ transition.

The gain dynamics described above may be better understood by examining the time histories of population for the vibrational levels in the B, C, and X states shown in Fig. 5. The conditions are the same as for Fig. 4. Note that the density of XeCl($B,v'=4$) exceeds that of $v'=2$ and 3. This condition results from formation of XeCl(B) occurring at high vibrational levels and the fact that vibrational relaxation to lower levels by collisions with the buffer gas has a relatively small rate ($\approx 2/5\times 10^{8}$ atm^{-1} s^{-1}) compared to the rate of depopulation of XeCl($B,v'=0$) by optical extraction. Even ignoring the population of XeCl($B,v'=4$), we find that the densities of XeCl($B,v'\leqslant 3$) are not in thermal equilibrium. The ratios of these densities are quite sensitive to the degree of B-C mixing. Laser oscillation begins at approximately 100 ns, as indicated by the saturation of XeCl($B,v'=0$). Saturation is also apparent on XeCl($B,v'=1$) as an indication of the coupling of $v'=1$ and $v'=0$ by upwards collisions. The saturation of XeCl($B,v'>1$) is barely discernable from the oscillations in population due to circuit ringing as a result of weak coupling of $v'>1$ with $v'=0$. The vibrational distribution in the C state monotonically decreases going to higher levels, though it is not in thermal equilibrium. Note that the amount of saturation of XeCl($C,v'\leqslant 2$) compares to that of the B state, as a result of fairly tight mixing between XeCl($B,v'=0$) and XeCl($C,v'=1$).

The populations of the vibrational levels in the X state clearly show the effects of saturation and bottlenecking. The densities shown in Fig. 5(c) are the departures from the thermal equilibrium and of the thermal equilibrium density of the X state. For these conditions $0\rightarrow 1$ and $0\rightarrow 2$ transitions are oscillating with approximately equal power. The densities of XeCl($X,v''=1$) and XeCl($X,v''=2$) exceed that of XeCl($X,v''=0$) and that of the equilibrium density. Even though the $0\rightarrow 2$ transition is somewhat more intense, the population of XeCl($X,v''=1$) exceeds that of XeCl($X,v''=2$) due to the effective downward cascade due to thermalization of $v''=2$ and because the rate of dissociation of $v''=2$ is larger than the rate of removal of $v''=1$. It is clear that bottlenecking on individual vibrational levels of XeCl(X) may occur for these conditions.

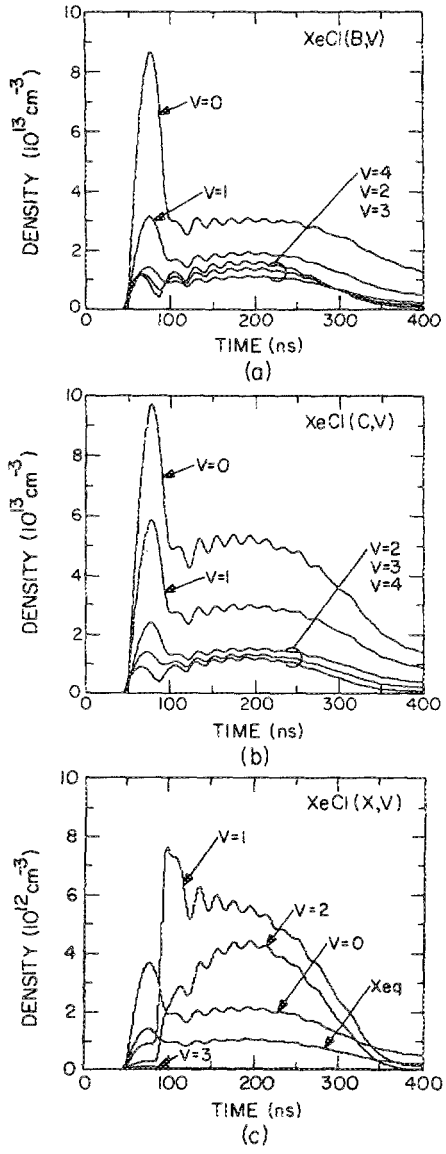

FIG. 5. Densities of the vibrational levels of (a) XeCl(B), (b) XeCl(C), and (c) XeCl(X) for the conditions of Fig. 4 (nonequilibrium kinetics in the X state). Laser oscillation begins on the $0\rightarrow 1$ and $0\rightarrow 2$ transitions at approximately 100 ns. The saturation of XeCl($B,v'=1$) and XeCl($C,v'=0,1,2$) indicates the tight coupling between these levels and XeCl($B,v'=0$). The large increase in XeCl($X,v''=1$) above the equilibrium value and XeCl($X,v''=0$) indicates bottlenecking.

IV. INJECTION-LOCKING CHARACTERISTICS

In this section the spectral characteristics of injection locking of XeCl($B\rightarrow X$) lasers will be discussed. The pumping and optical cavity parameters are the same as those of the free-running system discussed above. In the model we assume that radiation is uniformly injected into the laser cavity until the termination of laser oscillation. The injected signal is at the wavelength at which peak gain occurs on each band. The injection intensity is 200 kW/cm^2 unless otherwise noted and we assume that there are no intracavity dispersive elements. For purposes of comparison, we define the injection-locking efficiency as the fraction of laser energy obtained at the injected wavelength compared to the total laser energy.

Laser intensities when injecting on the XeCl($B\rightarrow X$) $0\rightarrow 1$, 2, and 3 transitions are shown in Fig. 6. For our conditions, injection locking cannot be obtained on the $0\rightarrow 0$ transition as its gain is too low. This is partially due to an effective downward cascade of vibrational population in the X state resulting from thermalization, the small rate of dissociation of $v''=0$ compared to higher levels, and smaller Franck–Condon factors. Injecting on $0\rightarrow 1$ successfully locks onto

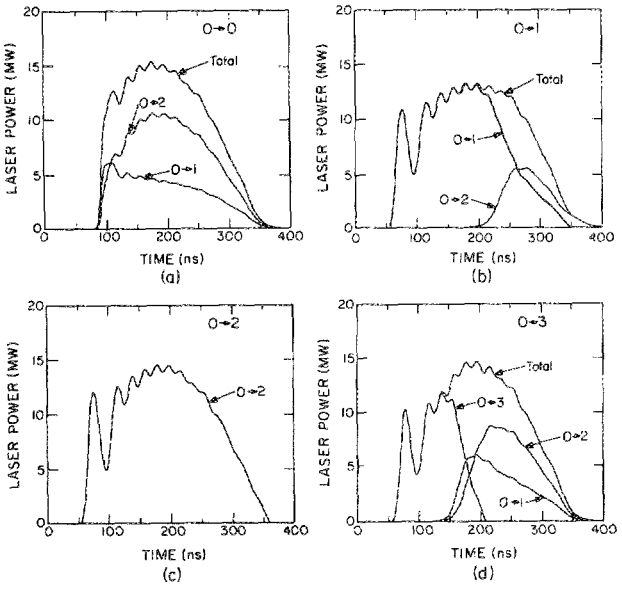

FIG. 6. Laser intensities for injection locking of the discharge excited XeCl($B \rightarrow X$) laser. The injection level is 200 kW cm^{-2} at the wavelength of maximum gain. Results are shown for injecting on the (a) 0→0, (b) 0→1, (c) 0→2, and (d) 0→3 transitions. Oscillation cannot be sustained on the 0→0 transition for these conditions so the laser oscillates with nearly its free running characteristics. Locking is only complete on the 0→2 transition while locking on the other transition is lost at later times during the pulse.

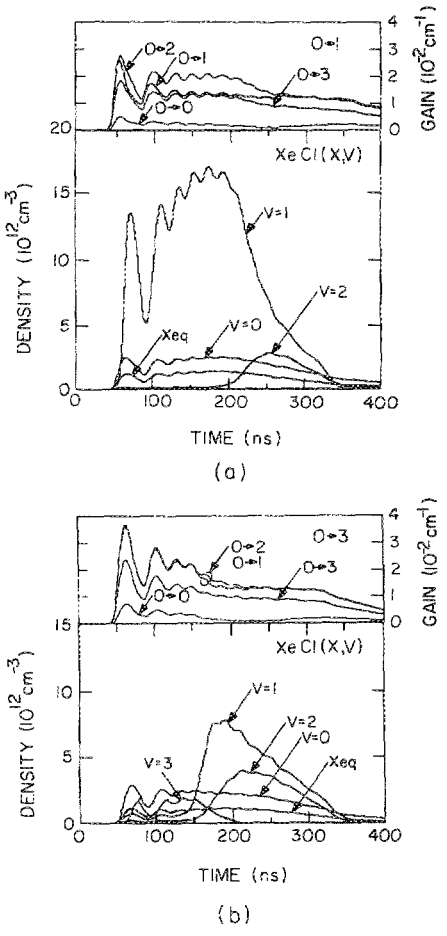

FIG. 7. Gain on the XeCl($B \rightarrow X$) transitions and densities of the vibrational levels in the X state for injection on the (a) 0→1 transition and (b) 0→3 transition.

that transition. Note that oscillation begins approximately 30 ns earlier than in the free-running laser due to the seeding of the cavity with the injected radiation. Injection on 0→1 transition does not provide permanent locking as the 0→2 transition builds from noise and begins to oscillate at $t \approx 200$ ns. The cause for the loss of spectral locking is primarily bottlenecking in the X state on $v'' = 1$, and the slightly higher oscillator strength of the 0→2 transition. The densities of the vibrational levels in the X state are shown in Fig. 7(a) for this case. Note that XeCl($X,v'' = 1$) is highly saturated and bottlenecked. The contribution to XeCl($X,v'' = 2$) from the thermal distribution is barely discernable prior to $t = 200$ ns. When the 0→2 transition begins to oscillate, the XeCl($X,v'' = 2$) density rapidly increases. The density of XeCl($X,v'' = 1$) does not dramatically decrease at this time in spite of a reduction in the 0→1 optical intensity due to its slower rate of removal. The locking efficiency when injecting on 0→1 for these conditions is 82%.

Injection on the 0→2 level results in locking with nearly 100% efficiency. Successful locking results from the somewhat higher oscillation strength of that transition and the small rate of downward transitions from higher vibrational levels in the X state, resulting from thermalization, which would lower gain. Also, the higher rate of dissociation of the XeCl($X,v'' = 2$) level averts significant bottlenecking.

When injecting on the 0→3 transition, locking is obtained for only half the length of the pulse after which the laser reverts to its free-running mode. The locking efficiency is 38%. Locking should be fairly efficient on this transition because of the lack of bottlenecking on XeCl($X,v'' = 3$). There is little effective cascade from higher levels due to thermalization and the rate of direct dissociation of XeCl($X,v'' = 3$) is higher than the lower vibrational levels. The higher rate of dissociation of $v'' = 3$, though, reduces the effective cascade to the lower vibrational levels, thereby not saturating those levels as shown in Fig. 7(b). As a result, oscillation on 0→1 and 0→2 transitions eventually builds from noise due to their higher oscillator strengths. Clearly injection efficiency is a function of pulse length and gain since, for example, total locking is obtained on the 0→3 transition for the first 100 ns. These issues are discussed in more detail below.

Locking efficiency as a function of wavelength is shown in Fig. 8 for the same pumping and optical cavity conditions as for Fig. 6. Locking efficiency based on total laser energy and locking efficiency based on laser power at $t = 150$ ns are plotted. For long pulses, represented by the efficiency based on total laser energy, total locking can only be obtained on the 0→2 transition. Away from the local peak in the gain distribution, locking efficiency falls to near zero. The power locking efficiency at the shorter pulse time is higher than the energy locking efficiency, however, locking can still not be obtained between the peaks of the gain profile. For these cases, wavelength dispersive or selective optics may be required. Clearly for transitions originating on the same level, the transition having the higher oscillator strength will eventually oscillate regardless of the intensity of the transition having the smaller oscillator strength unless there is selective population of the lower laser level for the stronger transition.

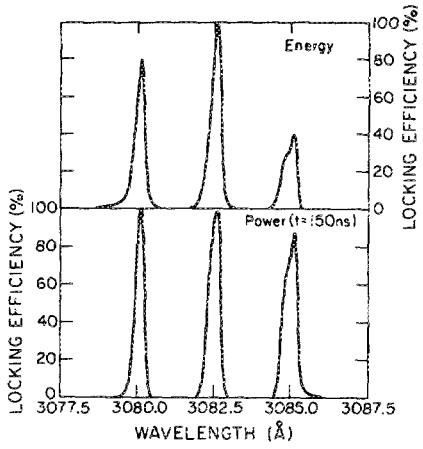

FIG. 8. Injection locking efficiency as a function of wavelength for an injected signal of 200 kW cm^{-2}. Locking efficiency based on total laser energy is shown at the top. Locking efficiency based on laser power at $t = 150$ ns is shown at the bottom.

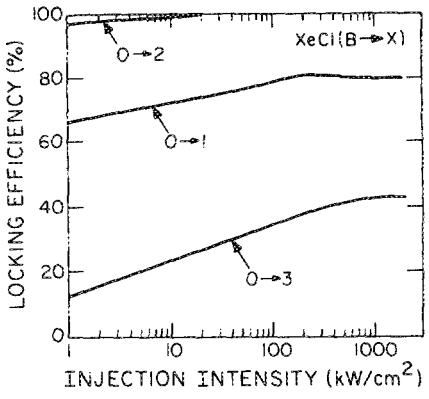

FIG. 9. Locking efficiency (based on total laser energy) as a function of injection power for the XeCl($B,v' = 0$)→XeCl($X,v'' = 1,2,3$) transitions.

Injection locking for a pulsed high gain laser with multiple transitions from a common upper level must therefore be transient.

Our results qualitatively agree with those of Bourne and Alcock[5] although they obtain higher locking efficiencies at off-peak wavelengths. Our results are consistent with those of Lyutskanov, Khristov, and Tomov[28] who could not obtain oscillation at the off-peak wavelengths when grating tuning on an XeCl laser. The differences between our results and those of Bourne and Alcock may be due to differences in the optical cavity and the shorter pulse lengths used by Bourne and Alcock.[5] Nevertheless, our off-peak gain coefficients are somewhat smaller than those required to obtain locking at all the wavelengths observed by Bourne and Alcock. We hypothesized that this condition is due to our approximate treatment of Franck–Condon factors as a function of rotational level. As values were only available for $J = 0$ and $J = 50$, we linearly interpolated between these values. We parametrized the spectral model using other dependencies without obtaining significantly different results. Therefore, to obtain higher off-peak gain than we calculate, either the rotational distribution must not be in equilibrium with the gas temperature or the spectroscopic constants are not accurate. We found that the ratio of gain between $0 \rightarrow 1$ and $0 \rightarrow 2$ transitions to be most sensitive to the Franck–Condon factors and the rotational constant. The width of the gain on a given transition is most sensitive to the rotational level above which fine splitting of the vibrational level is accounted for. This splitting is accounted for by the factor K in Eq. (10). We used $K = 1/4$ for $J_c \geqslant 20$. Larger values of J_c result in a wider gain spectrum.

If the Franck–Condon factors used in the model and reported by Sur, Hui, and Tellinghuisen[6] are significantly in error, then our conclusion concerning the necessity for bottlenecking in XeCl(X) to obtain injection locking could also be in error. Given that these spectroscopic constants are otherwise considered valid, our conclusion concerning bottlenecking must stand until the results of Sur and coworkers are revised or updated.

Locking efficiency is shown in Fig. 9 as a function of injection intensity for the same conditions as Fig. 6. Locking efficiency increases with increasing injection intensity until a value at which the locking efficiency saturates. This value for each transition is determined by the vibrational dynamics in the X state. The injection level at saturation is fairly high for the $0 \rightarrow 3$ transition due to rapid removal of population in XeCl($X,v'' = 3$). Again, these locking efficiencies are functions of pulse lengths.

V. DEPENDENCE OF LOCKING EFFICIENCY ON GAIN

Lean gas mixtures (i.e., low HCl fraction) are usually used for discharge-pumped XeCl lasers because more uniform discharges, and hence higher laser efficiency, can be obtained than with rich mixtures.[30] Higher gain, though, can be obtained with rich mixtures if the plasma remains homogeneous. Discharge stability issues aside, changing the HCl concentration does provide a convenient method to change the small-signal gain and to investigate the effect of small-signal gain on injection efficiency. We have performed such a study by changing the HCl concentration in our model, and observed the change in gain and injection locking. The HCl concentrations we examined should be within the range that the effect of discharge instabilities is small based on the experimental results reported so far.

A complicating factor in changing the HCl concentration is that in lean mixtures power loading may deplete the HCl during the pulse so that small-signal gain is not necessarily constant during the discharge. To decrease the effects of HCl depletion on the production of XeCl* a laser configuration was used in the model where energy loading is less than with the parameters used above. The pulse-forming line (PFL) of the new configuration has a characteristic impedance of 0.3 Ω and a double transit time of 58 ns. The discharge volume is 2 cm high by 1 cm wide by 60 cm long (120 cm^3). The optical cavity consists of a total reflector and a 20% reflectivity output mirror separated by 1 m. The laser head is connected to the PFL through a rail-gap switch and a peaking capacitor of 1 nF. The rail-gap switch is modeled as a constant inductance of 10 nH with a time-dependent series resistance which reaches 0.025 Ω with a 4-ns time constant after triggering. The calculated laser pulse width is ≈100 ns

in a free-running system. The laser output energy for the same gas mixture as used above (Ne/Xe/HCl = 99.47/0.5/0.03) is 315 mJ (2.6 J/ℓ) with an overall efficiency of 2.6%. The peak pumping density is 0.8 MW/cm^3 which for a 5-atm gas mixture does not result in significant burnup for the range of HCl concentrations we investigated.

Peak small-signal gain computed with the model for the device described above is shown in Fig. 10 as a function of HCl concentration. The small-signal gain for each vibrational transition is the peak value in the gain profile. The peak gain for each transition increases monotonically with increasing the HCl concentration. Gains at the high range of HCl concentrations may be optimistic due to questionable discharge stability at those values of HCl fraction. Large gains (>0.14 cm^{-1}), though, have been reported for wide aperture (2.8 cm$\times$3 cm) discharge lasers having HCl concentrations as high as 0.1%.[31]

Locking efficiencies are shown in Fig. 11 as a function of small signal gain for 200 kW cm^{-2} uniformly injected into the laser cavity for the conditions of Fig. 10. Locking efficiencies of the $0\rightarrow1$ and $0\rightarrow2$ transitions as a function of small-signal gain and injection intensity are shown in Fig. 12. Locking efficiency does not generally increase with increasing small-signal gain for other than the $0\rightarrow3$ transition. For small-signal gains of more than 0.05 cm^{-1}, the locking efficiencies saturate or decrease. This results from the fact that oscillation at other than that injected wavelength are initiated by spontaneous emission which increases with increasing gain. Threshold for the noninjected transitions is therefore reached sooner under conditions of higher gain. Locking efficiency decreases for these conditions even for an injection intensity on the order of the laser output intensity as shown in Fig. 12. Although the laser line at the injected wavelength builds up faster at higher values of small-signal gain, lines other than at the injected wavelength also grow faster from spontaneous emission.

By comparing locking efficiencies for the four vibrational transitions at the same small-signal gain, one can isolate the effects of ground state dynamics. At values of small-

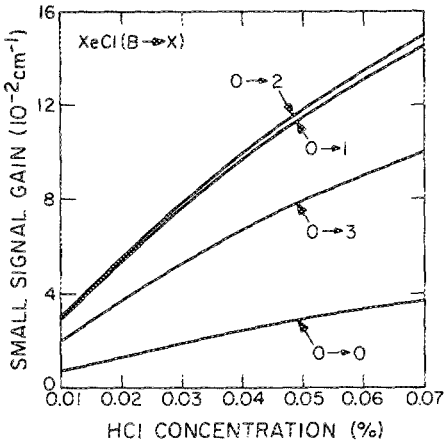

FIG. 10. Small-signal gain for the XeCl($B,v'=0$) $\rightarrow$ XeCl($X,v''=0,1,2,3$) transitions as a function of HCl concentration. These gains may be optimistic for high HCl concentration due to issues related to discharge stability which are not addressed in this model. The method nevertheless provides a method to investigate the effect of small-signal gain on locking efficiency.

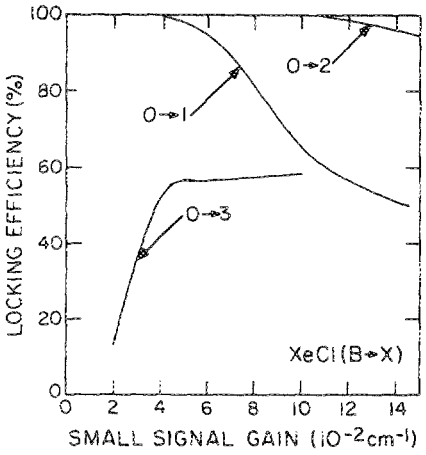

FIG. 11. Locking efficiency (base on total energy) for the XeCl($B,v'=0$) $\rightarrow$ XeCl($X,v''=0,1,2$) transitions as a function of small-signal gain for the conditions of Fig. 10. The locking efficiency of transitions terminating on the lower vibrational levels ($0\rightarrow1$, $0\rightarrow2$) decreases with increasing small-signal gain. This effect results, in part, from the cascading of population from transitions terminating on higher vibrational levels when those lines begin to oscillate. The $0\rightarrow3$ transition, not subject to this effect, has a locking effciency which increases with small-signal gain.

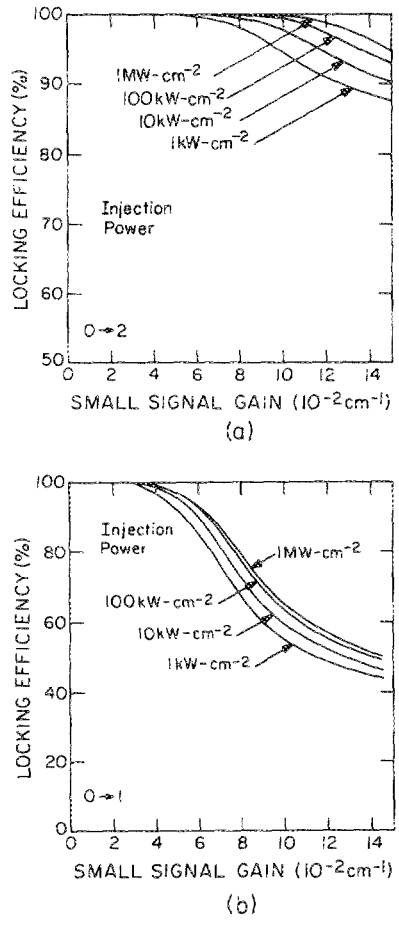

FIG. 12. Locking efficiency as a function of small-signal gain and injection intensity (1 kW cm^{-2} to 1 MW cm^{-2}) for the conditions of Fig. 11; (a) XeCl($B,v'=0$) $\rightarrow$ XeCl($X,v''=2$) and (b) XeCl($B,v'=0$) $\rightarrow$ XeCl($X,v''=1$). For these dominant transitions, the injection intensity has little effect on locking efficiency. Increasing the injection intensity is unable to compensate for the effects of ground-state dynamics which decrease locking efficiency with increasing small-signal gain.

signal gain $>0.05\ \mathrm{cm}^{-1}$, the locking efficiency of the $0\rightarrow 1$ transition decreases while that for the $0\rightarrow 3$ transition remains a constant. This results from differences in the removal rate of population from the vibrational levels in the X state. For example the direct dissociation rate of $\mathrm{XeCl}(X,v''=3)$ is higher than that of $\mathrm{XeCl}(X,v''=0,1,2)$. This level is also less susceptible to saturation by transitions terminating on lower levels. Therefore, one would expect that the $0\rightarrow 3$ transition would be somewhat favored at high gain over the transitions terminating on lower vibrational levels which are subject to cascading from higher levels, and which have a lower direct dissociation rate constant.

VI. INJECTION LOCKING AS A FUNCTION OF POSITION

As a result of nonuniformities in preionization density, electric field (due to electrode profiling), and halogen burnup, discharge parameters are generally not uniform as a function of position.[30,32,33] In particular, small-signal gain and the saturation intensity may be functions of position as results of differences in both the rate of pumping and the rate of quenching due to electrons. Therefore, when attempting to injection lock a discharge excited $\mathrm{XeCl}(B\rightarrow X)$ laser, the injection-locking efficiency may be a function of position.

To investigate locking efficiency as a function of position, we modified our discharge laser model to be a one spatial dimension simulation. The spatial dimension is parallel to the electrodes and perpendicular to the optical axis. We assumed that the discharge properties are not a function of position in the direction of the optical axis or perpendicular to the electrodes. In this formulation, the profile of the electrode and the spatial distribution of the preionization electron density may be specified. The resonator consists of plane-plane mirrors. The spatial aspects of this model are functionally equivalent to those described in Ref. 32.

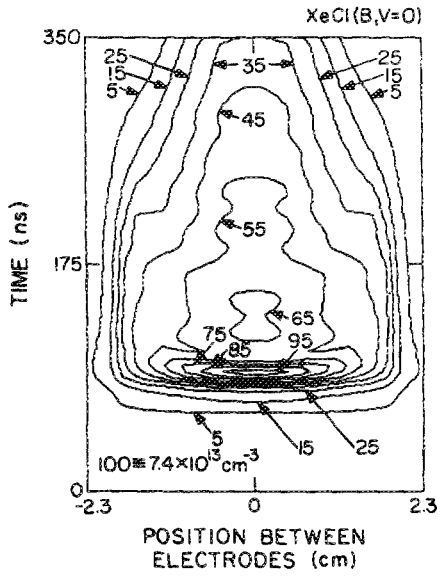

FIG. 13. Density of $\mathrm{XeCl}(B,v'=0)$ as a function of position and time for conditions similar to those for Fig. 6. Injection is on the $0\rightarrow 3$ transition at 200 kW cm^{-2}. The preionization density was chosen so that the discharge would constrict. The spatial dimension is across the face of the discharge parallel to the electrodes and perpendicular to the optical axis. The contour value of 100 corresponds to a maximum density of $7.4\times 10^{14}\ \mathrm{cm}^{-3}$.

To accentuate the effects of nonuniform discharge parameters on locking efficiency we chose conditions where the discharge would constrict by having a preionization electron density that peaks on the central axis. The conditions are otherwise the same as described above for the larger device. Discharge constriction results in a higher current density on the axis, which translates to higher pumping, more depletion of HCl, and higher electron quenching on the axis. The density of $\mathrm{XeCl}(B,v'=0)$ for these conditions is plotted in Fig. 13 as a function of position between the electrodes and time. The injection signal is for the $0\rightarrow 3$ transition. The $\mathrm{XeCl}(B,v'=0)$ density rises fairly uniformly as a function of position early during the pulse, but then as constriction begins the density of $\mathrm{XeCl}(B,v''=0)$ is highest on the axis.

Laser power is plotted in Fig. 14 while injecting uniformly on the $0\rightarrow 3$ transition for the same conditions as in Fig. 13. The time dependencies of laser power on the axis ($x=0$) for the $0\rightarrow 1$, 2, and 3 transitions are shown in Fig. 14(a). The laser goes out of lock at approximately 150 ns. The time- and spatially dependent laser powers for the $0\rightarrow 3$ and $0\rightarrow 1$ transitions are shown in Fig. 14(b). The $0\rightarrow 3$ transition turns on fairly uniformly across the face of the dis-

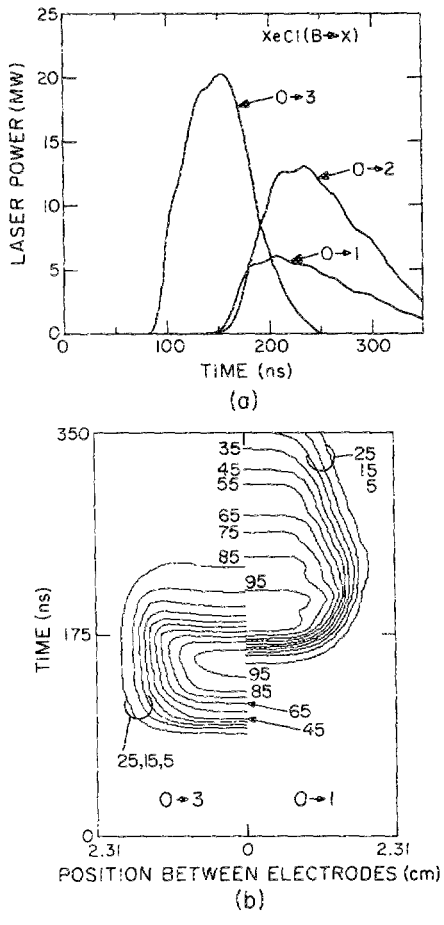

FIG. 14. Laser power while injecting on the $0\rightarrow 3$ transition for the conditions of Fig. 13; (a) laser power on axis and (b) laser power for the $0\rightarrow 3$ and $0\rightarrow 1$ transitions as a function of position and time. As the discharge parameters are symmetric across the center line, we plotted laser power for only one side of the discharge for each laser line. The $0\rightarrow 3$ transition turns on fairly uniform across the face of the discharge. The $0\rightarrow 1$ transition oscillates first on the axis and later at the edges of the discharge.

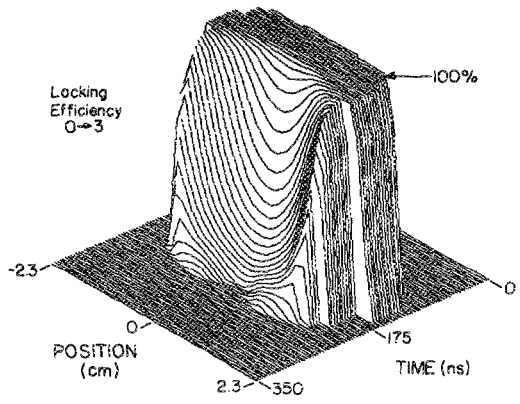

FIG. 15. Locking efficiency on the 0→3 transition (based on instantaneous fractional laser power) as a function of position and time for the conditions of Fig. 14. The laser goes out of lock first on the axis and later at the edge of the discharge. Note that the time axis goes from the rear to the front of the figure.

charge, however, the 0→1 transition turns on first on the axis and later towards the edge of the discharge. As pumping is higher on the axis due to the constriction at later times, laser power also constricts towards axis late in the pulse. Locking efficiency for the 0→3 transition is shown in Fig. 15 as a function of position and time for the same conditions. The laser goes out of lock first on the axis and later at the edge of the discharge. The small decrease in net small-signal gain for the 0→3 transition, and the increase in saturation intensity for the 0→3 transition on the axis resulting from a higher rate of electron collision quenching, allows the 0→1 and 0→2 transitions to oscillate there first. Off axis, where the saturation intensity is higher, the laser remains in lock for a longer time.

VII. CONCLUDING REMARKS

Laser spectra of discharge-pumped XeCl($B \rightarrow X$) lasers have been theoretically investigated by using a kinetic model for Ne/Xe/HCl/H_2 mixtures which includes the gain spectrum calculated based on the Franck–Condon factors.[6] The model also vibrationally resolves the B, C, and X states. We find that the vibrational distribution of the X state is far from being in thermal equilibrium with the gas temperature. This condition is attributed to slow removal rates out of the lowest vibrational levels. The removal rate of the XeCl($X,v''=1$) is $\approx 1\times 10^{-11}$ cm^3 s^{-1} for Ne buffers and leads to bottlenecking on the 0→1 transition. The direct dissociation rate of XeCl($X,v''=2$) is faster than the removal rate of $v''=1$ and this condition explains the nearly equal division of laser energy (in a free-running oscillator) between the 0→1 and 0→2 transitions as reported by Bourne and Alcock.[5] Furthermore, the fact that locking efficiency does not necessarily increase with increasing small-signal gain is largely a result of saturation effects in the ground state.

ACKNOWLEDGMENTS

This work was funded in part by General Dynamics Laser Division and Los Alamos National Laboratory.

[1]P. C. Tellinghuisen, J. Tellinghuisen, J. A. Coxon, J. E. Velazco, and D. W. Setser, J. Chem. Phys. **68**, 5187 (1987).
[2]J. Tellinghuisen, J. M. Hoffman, G. C. Tisone, and A. K. Hays, J. Chem. Phys. **64**, 2484 (1976).
[3]S. F. Fulghum, M. S. Feld, and A. Javan, Appl. Phys. Lett. **35**, 247 (1979).
[4]P. B. Corkum and R. S. Taylor, IEEE J. Quantum Electron. **QE-18**, 1962 (1982).
[5]O. L. Bourne and A. J. Alcock, Appl. Phys. Lett. **42**, 777 (1983).
[6]A. Sur, A. K. Hui, and J. Tellinghuisen, J. Mol. Spectrosc. **74**, 465 (1979).
[7]R. W. Waynant and J. G. Eden, Appl. Phys. Lett. **36**, 262 (1980).
[8]M. Maeda, A. Takahashi, T. Mizunami, and Y. Miyazoe, Jpn. J. Appl. Phys. **21**, 1161 (1982).
[9]F. Kannari, A. Suda, M. Obara, and T. Fujioka, IEEE J. Quantum Electron. **QE-19**, 1587 (1983).
[10]C. H. Fisher, M. J. Kushner, T. E. DeHart, J. P. McDaniel, R. A. Petr, and J. J. Ewing, Appl. Phys. Lett. **48**, 1574 (1986).
[11]M. Ohwa and M. Obara, J. Appl. Phys. **59**, 32 (1986).
[12]H. Hokazono, K. Midorikawa, M. Obara, and T. Fujioka, J. Appl. Phys. **56**, 680 (1984).
[13]T. H. Johnson, L. J. Palumbo, and A. M. Hunter, II, IEEE J. Quantum Electron. **QE-15**, 289 (1979).
[14]T. G. Finn, R. S. F. Chang, L. J. Palumbo, and L. F. Champagne, Appl. Phys. Lett. **36**, 789 (1980).
[15]G. C. Tisone and J. M. Hoffman, IEEE J. Quantum Electron. **QE-18**, 1008 (1982).
[16]T. D. Dreiling and D. W. Setser, J. Chem. Phys. **75**, 4360 (1981).
[17]A. Kvaran, M. J. Shaw, and J. P. Simons, Appl. Phys. B **46**, 95 (1988).
[18]P. J. Hay and T. H. Dunning, J. Chem. Phys. **69**, 2209 (1978); T. H. Dunning and P. J. Hay, J. Chem. Phys. **69**, 434 (1978).
[19]J. Tellinghuisen and M. R. McKeever, Chem. Phys. Lett. **72**, 94 (1980).
[20]H. C. Brashears, Jr., D. W. Setser, and Y. C. Yu, J. Chem. Phys. **74**, 10 (1980).
[21]D. Lo and C.-E. Zheng, J. Phys. D **20**, 717 (1987).
[22]C. H. Fisher, R. E. Center, and J. J. McDaniel, presented at 32nd Annual Gaseous Electronics Conference, Pittsburgh, PA, October 1979 (unpublished).
[23]G. Inoue, J. K. Ku, and D. W. Setser, J. Chem. Phys. **80**, 6006 (1984).
[24]D. W. Setser, H. C. Brashears, and T. D. Dreiling, J. Phys. (Paris) Colloq. **41**, C3-195 (1980).
[25]W. H. Long, Jr., M. J. Plummer, and E. A. Stappaerts, Appl. Phys. Lett. **43**, 735 (1983).
[26]A. N. Adkhamov, B. A. Azimdzhanov, T. U. Arslanbekov, V. I. Mikhailov, A. N. Obichkin, I. M. Ternovskii, and V. E. Chekalin, Sov. J. Quantum Electron. **18**, 72 (1988).
[27]V. A. Adamovich, V. Yu. Baranov, A. A. Deryugin, I. V. Kochetov, D. D. Malyuta, A. P. Napartovich, Yu. B. Smakovskii, and A. P. Strel'tsov, Sov. J. Quantum Electron. **17**, 45 (1987).
[28]V. L. Lyutskanov, Kh. G. Khristov, and I. V. Tomov, Sov. J. Quant. Electron. **10**, 1456 (1980).
[29]S. F. Fulghum, M. S. Feld, and A. Javan, IEEE J. Quantum Electron. **QE-16**, 815 (1980).
[30]R. S. Taylor, Appl. Phys. B **41**, 1 (1986).
[31]S. Watanabe, A. J. Alcock, K. E. Leopold, and R. S. Taylor, Appl. Phys. Lett. **38**, 3 (1981).
[32]M. J. Kushner, A. L. Pindroh, C. H. Fisher, T. A. Znotins, and J. J. Ewing, J. Appl. Phys. **57**, 2406 (1985).
[33]M. J. Kushner and A. L. Pindroh, J. Appl. Phys. **60**, 913 (1986).